Journal of Materials Chemistry A

Accepted Manuscript

ROYAL SOCIETY OF CHEMISTRY

www.rsc.org/materialsA

Journal of
Materials Chemistry A

PAPER

Novelly developed three-dimensional carbon scaffold anodes from polyacrylonitrile for microbial fuel cells

Ya-Qiong Wang,[a] Han-Xiong Huang,[*a] Bin Li[b] and Wei-Shan Li[b,c]

Cite this: DOI: 10.1039/x0xx00000x

Received 00th xx 2014,
Accepted 00th xx 2015

DOI: 10.1039/x0xx00000x

www.rsc.org/MaterialsA

Performance and cost of anodes are two important aspects limiting the power output of microbial fuel cells (MFCs) for practical applications. Novel three-dimensional (3D) open-celled carbon scaffolds (CS and CS-GR) anodes were prepared by carbonizing the microcellular polyacrylonitrile (PAN) and PAN/graphite composites (PAN-GR), which were obtained by means of foaming via using supercritical carbon dioxide (Sc-CO_2) as physical foaming agent. The two anodes as well as conventional carbon felt anode were assembled in MFCs based on *Escherichia coli* (*E. coli*), respectively. The improved performance for the CS anode is ascribed to remained –C=N group resulting in considerably improved hydrophilicity and biocompatibility after carbonization and the 3D open-celled scaffold structure contributing to the substrate transfer and internal colonization of *E. coli* bacteria. Meanwhile, the superior performance for the CS-GR anode is mainly attributed to increased specific surface area and active reaction area resulting from the addition of graphite. This work provides an effective method to develop a 3D open-celled biocompatible CS-GR anode, which facilitates the extracellular electron transfer for high-performance MFCs that are promising for practical applications on a large scale.

[a]*Lab for Micro Molding and Polymer Rheology, The Key Laboratory of Polymer Processing Engineering of the Ministry of Education, South China University of Technology, Guangzhou, 510640, China. Email: mmhuang@scut.edu.cn; Fax: +8620 22236799*
[b]*School of Materials Science and Engineering, South China University of Technology, Guangzhou, 510640, China*
[c]*School of Chemistry and Environment, South China Normal University, Guangzhou, 510006, China*

1. Introduction

Microbial fuel cells (MFCs) are "green" energy-generating devices, in which chemical energy is directly converted into electrical energy by the electrocatalytic activity of electroactive bacteria.[1] Due to their broad range of potential applications, including marine sediment and wastewater treatments, home electrical generation, resource recovery, biosensing, and electronic power sources for space shuttles and self-feeding robots,[2–13] an exponential rise in research activities during the past few years has resulted in a remarkable growth in this field.[14]

Basic operation of MFCs is similar to that of other fuel cells (as shown in Fig. S1). The electrons produced by the oxidation of substrate at anode release to a cathode where an oxidant, such as oxygen, is reduced by passing through an external circuit.[15] The oxidation is associated crucially with the electroactive bacteria to form conductive biofilm, and the extracellular electrons are directly transferred to the electrode via three paths,[16] that is, microbial wall with redox-active outer membrane cytochromes, nanowires generated by bacteria, and diffusion of redox-active electron shuttles metabolized by bacteria (shown in Fig. S1). The performance of MFCs is dominated by electroactive bacteria indicated by intensive biofilm at anodes. So, the anode material as the medium of electron transfer and the support for biofilm formation is a key factor in determining their performance. Generally, anode material with larger specific surface area and higher affinity for bacteria adhesion provides MFCs with better performance.

Commercially available conventional carbon materials, such as graphite rod,[17] carbon cloth,[18] carbon paper,[19] carbon felt,[20] and reticulated vitreous carbon (RVC),[19] are widely used as anodes in MFCs in recent researches. The graphite rod is one of the most commonly employed anodes in MFCs, due to its excellent electrical conductivity and chemical stability. Liu et al.[21] carried out a representative research, in which the maximum power density is up to 26 mW m^{-2} in a single-chamber MFC using eight graphite rod anodes. However, the application of the graphite rod is limited due to its low porosity for bacteria adhesion. Lovely et al.[22] discovered that the power density is much higher when the graphite rod is replaced by the carbon felt, indicating that larger surface specific area contributes better performance to the MFCs. However, bacteria are inaccessible to the interior of the flat anodes. Thus, three-dimensional (3D) porous materials possessing open-celled microcellular structure for substrate transfer and internal bacteria colonization to improve extracellular electron transfer from bacteria to anode are being developed for high-performance MFCs. Examples include carbon nanotube-coated sponges,[23] graphene-coated sponges,[24] and polyaniline-hybridized graphene foams.[25] However, the problems associated with these 3D anodes lie in low biocompatibility,[25] high biodegradability of the supporting sponges,[26] and high costs due to the use of nanomaterials.[23]

To improve the biocompatibility, extensive studies have been devoted to altering the anode surface properties by surface treatment procedures, such as ammonia treatment that is beneficial to the bacteria adhesion for forming conductive biofilm due to the existence of nitrogen,[1,27] and heat and acid treatment for adding hydrophilic functional groups.[28–30] In addition, direct carbonization of available low cost materials provides a potential alternative to highly biodegradable supporting sponge anodes. Thus, besides high conductivity, chemical stability, and high specific surface area, the optimal anode with hydrophilic functional groups for biocompatibility and 3D open-celled scaffold is deemed preferable for MFCs, and clever design of the anode structure and careful cost-efficient selection of the anode materials are necessary.

Recently, Baranitharan et al.[31] investigated the performance of double chamber MFC using polyacrylonitrile (PAN) carbon felt as electrode in anode and cathode chambers. SEM observation on the anode conducted before and after operation in MFC demonstrated that bacteria of different sizes and shapes are scattered around the electrode, associated with a biofilm formed on its surface. Presence of

biofilm only on the electrode surface undoubtedly results in low electric conductivity and so suppresses the extracellular electron transfer. In this work, we developed a novel 3D carbon scaffold (CS) anode combining its open-celled scaffold structure with hydrophilic functional –C=N group for internal bacteria colonization and reversibility for improved extracellular electron transfer. PAN was used as a precursor, which possesses a particular characteristic that its thermal-decomposition temperature (220 °C) is obviously lower than its melting point (320 °C). Aiming at reducing the cost and achieving carbon yield to a large extent,[32,34] a foaming technology via using supercritical carbon dioxide (Sc-CO_2) as physical foaming agent was applied. To further improve the specific surface area, PAN/graphite (GR) composites was used as a precursor for preparing CS-GR anode. The prepared CS and CS-GR anodes were assembled in single-chamber MFC, and the reason for superior performance of the MFC with CS-GR anode was illustrated.

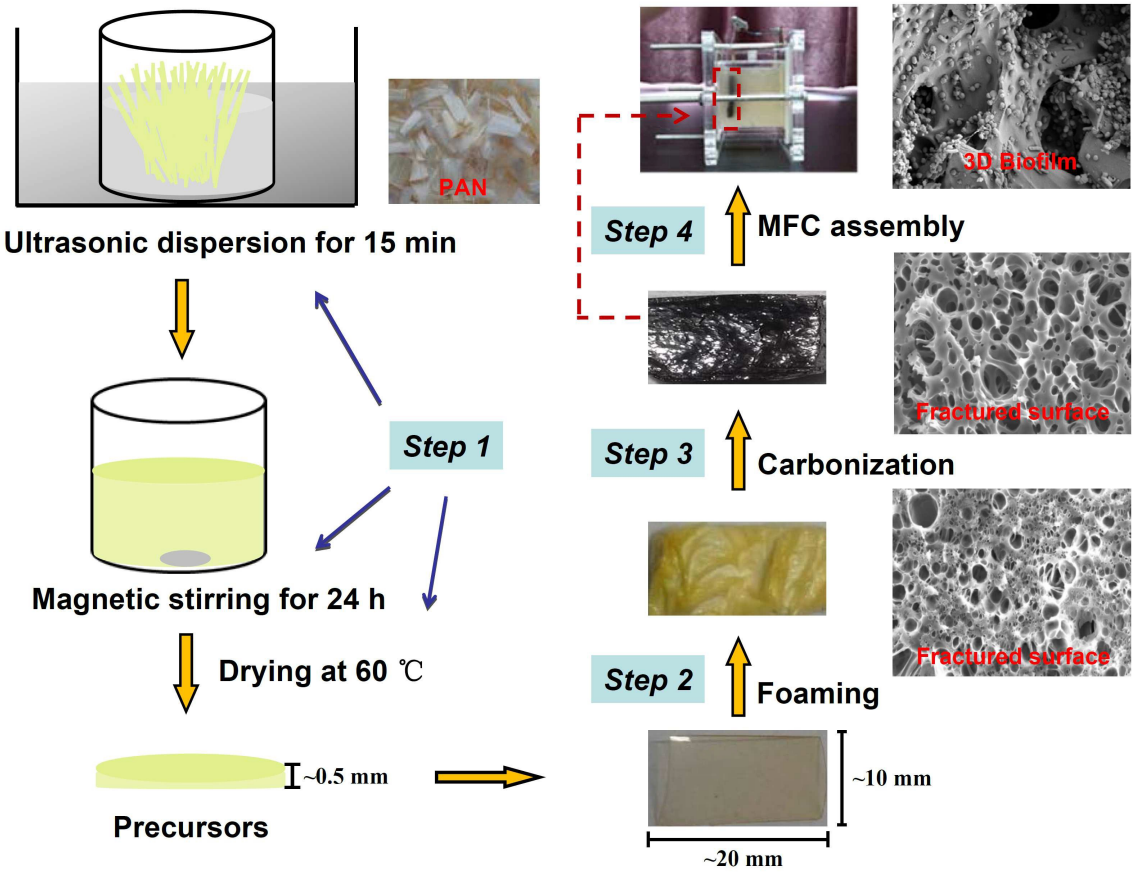

Fig. 1 Schematics of 3D open-celled carbon scaffold anodes preparation and MFC assembly.

2. Experimental

2.1 Materials

In this work, the polymer used was industrial grade PAN (Mw = 150000, Binzhou Jianbang Chemical Fiber Products Co., Ltd, China). The GR was purchased from Qingdao Zhongtian Graphite Co., Ltd, China. The solvent was dimethylsulfoxide (DMSO) (analytical grade, Sigma-Aldrich, USA).

2.2 Preparation and Assembly

The carbon scaffold anodes were prepared and assembled in MFCs through four steps as shown in Fig. 1.

Step 1. Precursor preparation

Two kinds of uniform precursor solutions were prepared by ultrasonically dispersing 10 wt% PAN and 10 wt% PAN plus 2 wt% GR evenly, respectively, in 5 mL DMSO solvent for 15 min at room temperature and then magnetic stirring gently for 24 h. Followed by drying at 60 °C overnight, both PAN and PAN-GR precursors with a thickness of about 0.5 mm were obtained.

Step 2. Microcellular PAN and PAN-GR preparation

The aforementioned PAN and PAN-GR precursors were cut into specimens with a size of about 20 mm×10 mm. The specimens were foamed by using Sc-CO_2 as physical foaming agent in a batch foaming apparatus via a pressure quenching manner. The batch foaming apparatus consisted of a high-pressure vessel and a syringe pump (ISCO 500D).[35,36] The vessel was heated to 200 °C and then the specimens were placed in the vessel. The vessel was slowly flushed with low-pressure CO_2 for 1 min to remove the air and then pressurized to the foaming pressure (20 MPa). Once the vessel pressure reached 20 MPa, the timing began. Followed by saturating the specimens at 20 MPa and 200 °C for 5 h, the vessel pressure was released at a high depressurization rate of about 60 MPa s^{-1}. Finally, the foamed specimens were removed from the vessel to obtain microcellular PAN and PAN-GR samples, the thicknesses of which were about 2 mm.

Step 3. Carbon scaffold preparation

The microcellular PAN and PAN-GR samples underwent a carbonization process, that is, stabilization in air at 230 °C for 5 h in a tube furnace, carbonization at 500 °C in N_2 for 4.5 h at a heating rate of 10 °C min^{-1}, and complete carbonization at 1000 °C in N_2 for 4.5 h (shown in Fig. S2). Then two kinds of carbon scaffolds with similar sizes to those of the microcellular PAN and PAN-GR samples were obtained, which were denoted by CS and CS-GR samples, respectively.

Step 4. Electrode preparation and MFC assembly

The above-prepared CS and CS-GR samples were polished to a size of about 20 mm×10 mm×1 mm for preparing anodes for MFCs. Conventional carbon felt anode with the same size was also prepared for comparison. The anode was placed close to one inside wall of a polymethyl methacrylate chamber (30 mm×30 mm×20 mm) and a membrane cathode assembly (MCA) was fixed on its opposite wall. Then a cubic MFC was assembled. The MCA was prepared by hot-pressing carbon paper (10 mm×10 mm) on one side of a cation exchange membrane. The carbon paper was previously pasted with 0.3 mg cm^{-2} commercial Pt-catalyst (20 wt % Pt/C) in a mixture of polyvinylidene fluorine by a weight ratio of 65:15 in 0.8 mL N-methyl-2-pyrrolidone as previous report.[34]

The as-assembled MFC was washed with 1 mol L^{-1} HCl and 1 mol L^{-1} NaOH to remove possible metal and biomass contamination, and was rinsed by sterile water. To initiate the MFC test, its chamber was inoculated with 3 mL bacteria suspension at 37 °C in a constant temperature incubator (HPG-280 H, China). Then 10 mL anolyte, that is, phosphate-buffered basal medium (PBBM) with 2g L^{-1} glucose as fuel, was injected into the chamber. The PBBM consisted of 5.8 g NaCl, 0.1 g KCl, 0.25 g NH_4Cl, 10 mL vitamin solution, 10 mL trace mineral solution and phosphate buffer (50 mM, pH 7.0) per 1 L.

2.3 Characterization

The microcellular PAN and PAN-GR samples and the CS and CS-GR samples were immersed in liquid nitrogen for about 10 min and fractured. Then they were gold sputtered and their fractured surfaces were examined using scanning electron microscope (SEM, Quanta 200, FEI, Eindhoven, Holland). The specific surface area and pore volume of the CS, CS-GR, and carbon felt were determined using Brunauer–Emmett–Teller (BET) method on an ASAP 2400 Micromeritics (Atlanta, GA, USA), in which N_2 adsorption at 77K was applied. Before the measurements, the samples were degassed at 400 °C for 24 h in vacuum drying oven. The extent of carbonization was determined by detecting the disappearance of the characteristic groups in the microcellular PAN and PAN-GR samples before and after carbonization collected by means of fourier transform infrared spectroscope (FTIR,

BRUKER TENSOR27, Germany). The static water contact angles (CAs) on anode surfaces were measured via an optical contact angle measuring system (Dataphysics OCA 40, Germany). The volume of the droplet was set at 4 μL. The biofilms on the surfaces of the CS, CS-GR, and carbon felt anodes were observed using field-emission-type scanning electron microscopy (FESEM, ZESISS ULTRA 55, Germany).

2.4 Electrochemical measurements

Cyclic voltammograms (CVs), electrochemical impedance spectroscopy (EIS), and polarization tests were performed with a potentiostat (Autolab PGSTAT 30, Holland). The CVs tests were carried out with an Ag/AgCl (saturated KCl solution) as the reference electrode and platinum foil counter electrode in a three electrode configuration to investigate the electrochemistry characteristics of the CS and CS-GR anodes using 5 mM $K_3Fe(CN)_6$ prepared in 100 mM KCl buffer at a scan rate of 30 mV s^{-1}. Five circles were run for the CVs tests. The EIS tests were carried out in a frequency range of 100 kHz to 0.1 Hz with a signal of 10 mV amplitude. Anode impedance spectra were recorded using the anode as the working electrode and the cathode as the counter electrode in an anolyte with anaerobic culture of *Escherichia coli* (*E. coli*) bacteria. Power density curves were obtained by linear sweep voltammetry (scan rate 1 mV s^{-1}) with the potentiostat from the open circuit potential to 0 V. Before the measurement, the MFC was kept for one week till a stable voltage output was achieved. Three parallel tests were conducted. Power density was normalized to the apparent area (2.0 cm^2) of the anodes. The total internal resistance was obtained from the data of power density curves. Before each test, the chamber was purged over nitrogen for 15 min to remove oxygen from the solution.

3. Results and discussion

3.1 Porous structure and FTIR spectra of microcellular samples before and after carbonization

Fig. 2 illustrates the SEM micrographs of the microcellular PAN and PAN-GR samples and the CS and CS-GR samples to get an insight into their structures. As can be clearly seen, the microcellular PAN sample exhibits a nonuniform cell distribution, the mean diameters of large and small cells are about 5 and 0.5 μm, respectively (shown in Fig. 2(a)). The microcellular PAN-GR sample exhibits more uniform porous structure with a mean cell diameter of about 0.5 μm (Fig. 2(b)). After carbonization, the colour of the microcellular PAN and PAN-GR samples changes from beige to black, which means the formation of the ladder ring structure due to cyclization of the nitrile groups.[37,38] It is worth noting that the CS sample has a 3D open-celled scaffold structure with a mean diameter of about 5 μm (Fig. 2(c)), which is expected to allow the substrate transport and internal colonization of *E. coli* bacteria for facilitating the extracellular electron transfer from bacteria to the anode. The mean cell diameter of the CS-GR sample is about 2.5 μm (Fig. 2(d)), which is not expected to hinder the internal colonization of *E. coli* bacteria. The measured specific surface areas of the carbon felt and the CS and CS-GR samples are shown in Table 1. The CS sample has a large specific surface area of 4.69 m^2 g^{-1}, which is larger by about 13 times than that of the carbon felt. The CS-GR sample owns the maximum specific surface area (15.0 m^2 g^{-1}), 2-fold larger than that of the CS sample. Moreover, the CS-GR sample exhibits a larger total pore volume than the CS sample. So, the addition of the GR into the PAN precursor solution results in a significant increase in the specific surface area and porosity of the resultant scaffold, which is expected to provide high performance for MFCs.

The representative FTIR spectra of the microcellular PAN and PAN-GR samples and the CS and CS-GR samples are shown in Fig. 3. As is seen in Fig. 3(a), for the microcellular PAN sample, the prominent peaks at 1650, 2240, and 2940 cm^{-1} are assigned to the stretching vibrations of the –C=N, –C≡N, and –CH groups, respectively; whereas the peak at 1452 cm^{-1} corresponds to the bending vibration of $–CH_2$ group. For the CS sample, the peaks at 1452, 2240, and 2940 cm^{-1} disappear due to the elimination, cyclisation, and aromatization reactions occurring during the carbonization.[38] Of particular interest is the disappearance of the characteristic

peak at 2240 cm^{-1}, which confirms successful carbonization. Whereas the –C=N group at 1650 cm^{-1} is remained, which is expected to enhance the biocompatibility of the carbon scaffold originated from nitrogen dopant in it.[39] The FTIR spectra for the microcellular PAN-GR sample and the CS-GR sample have similar characteristics to those for the microcellular PAN sample and the CS sample, respectively (shown in Fig. 3(b)).

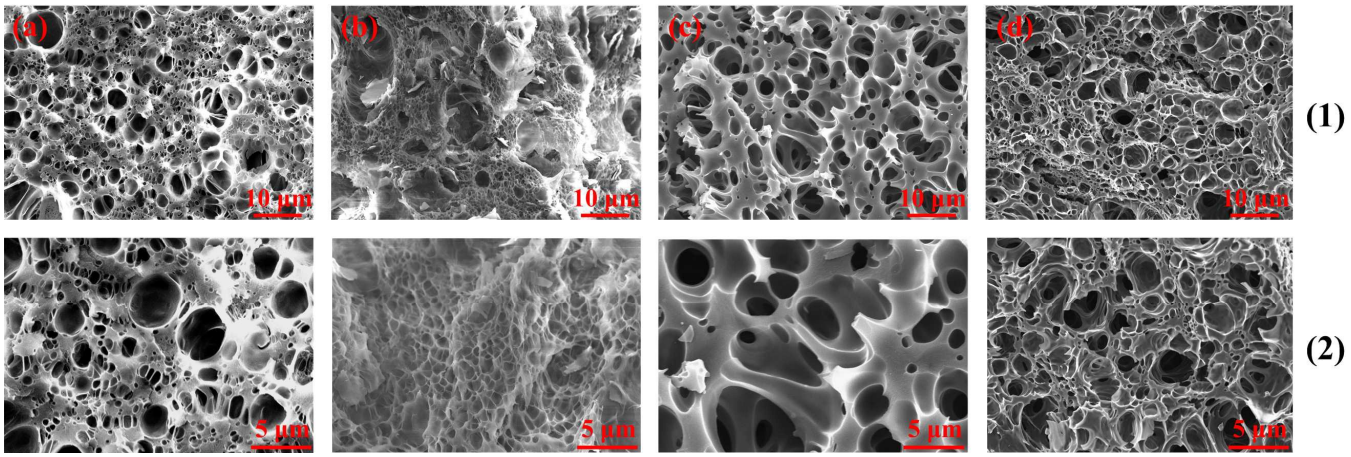

Fig. 2 SEM micrographs with (1) low and (2) high magnifications for microcellular (a) PAN and (b) PAN-GR samples, and (c) CS and (d) CS-GR samples.

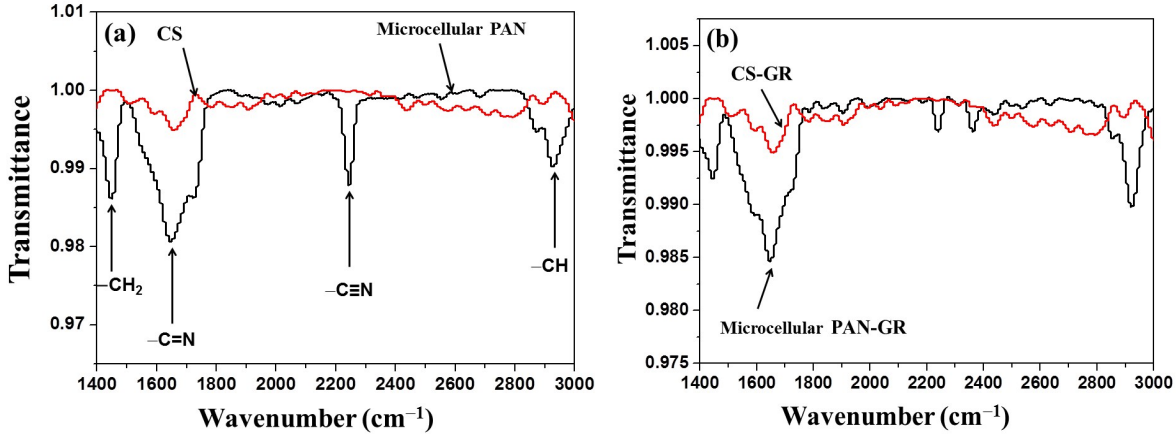

Fig. 3 FTIR spectra of microcellular PAN and PAN-GR samples, and CS and CS-GR samples.

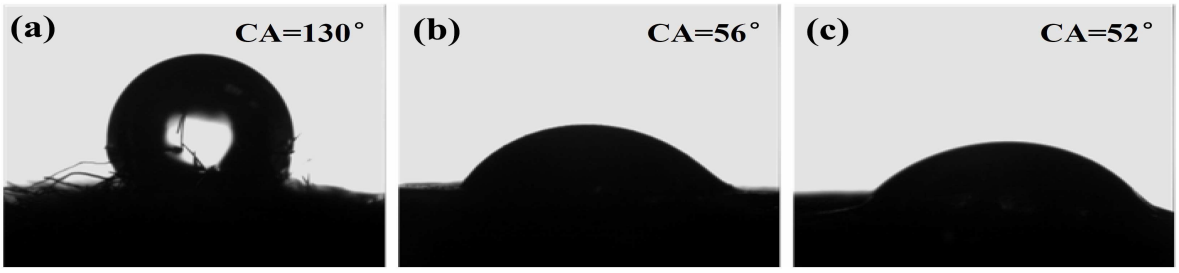

Fig. 4 Images of water droplets on (a) carbon felt, (b) CS, and (c) CS-GR anode surfaces.

Table 1 Specific surface area and porosity of different anodes

Anode	Specific surface area ($m^2\ g^{-1}$)	Total pore volume ($cm^3\ g^{-1}$)
Carbon felt	0.33	0.077
CS	4.69	1.08
CS-GR	15.10	3.46

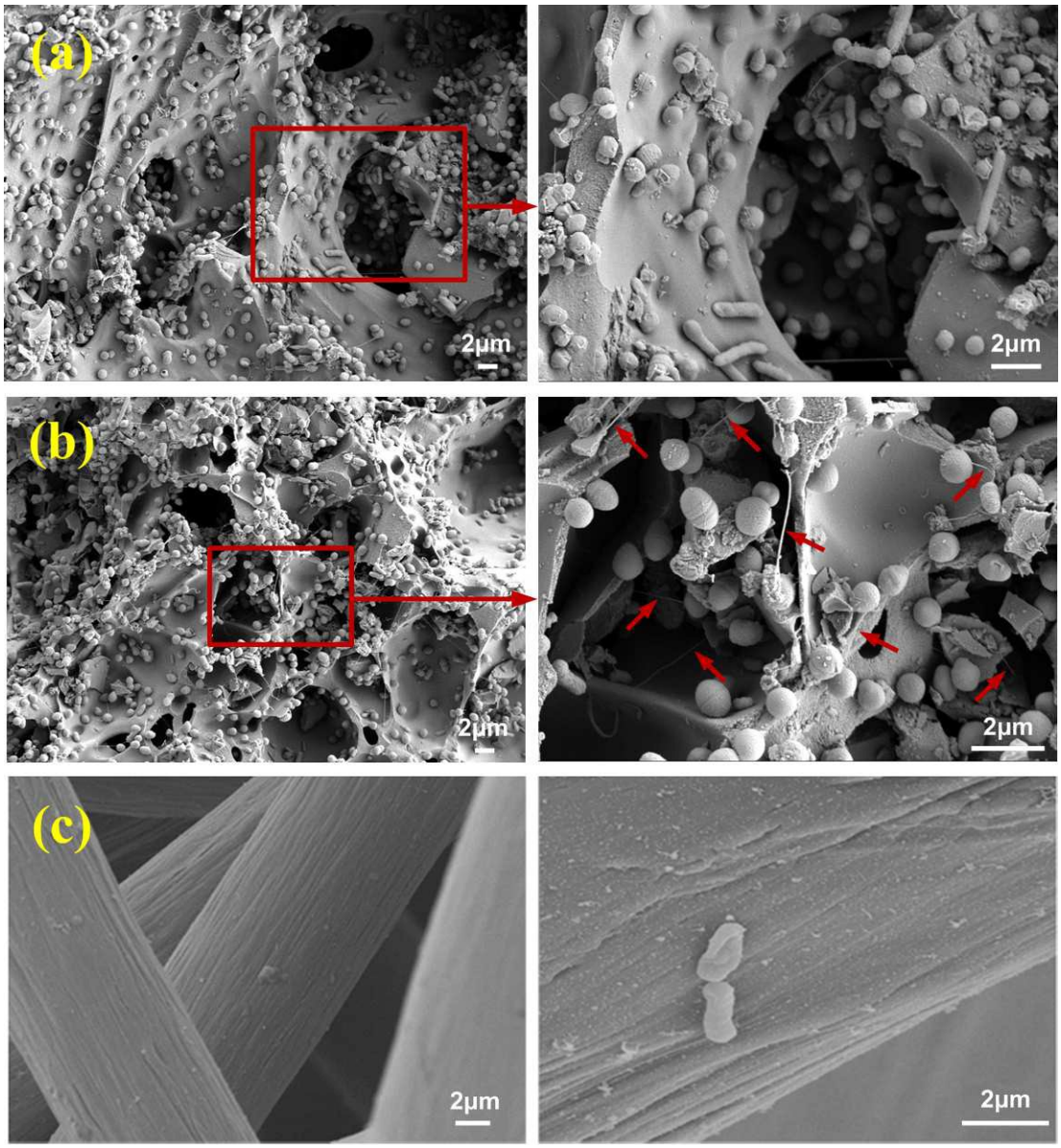

Fig. 5 FESEM micrographs of bacteria growth in (a) CS, (b) CS-GR, and (c) carbon felt anodes.

3.2 Biocompatibility and reversibility of anodes

The biocompatibility of the anode is determined by the hydrophilicity on its surface and is mainly embodied by the easiness of biofilm formation, which is responsible for the direct electron transfer between bacteria and anode in MFCs. The hydrophilic properties on the carbon felt, CS, and CS-GR anode surfaces were measured and the results are shown in Fig. 4, in which the CAs of water on anode surfaces are also given. The CA on the carbon felt anode is 130°, which demonstrates that the water can not spread well on the carbon

felt surface due to hydrophobic property of carbon material and jacking-up of the carbon fibre. It is worth noting that the CAs on the CS and CS-GR anodes are 56° and 52°, respectively. Obviously smaller CAs on the two anodes indicate that the remained –C=N group after the carbonization (as shown in Fig. 3) improves their hydrophilicities. Moreover, the 3D open-celled scaffold structure likely results in the infiltration of water facilitating the substrate transfer and internal colonization of bacteria, which will be analyzed in the next section.

Fig. 5 gives the FESEM micrographs of the bacteria growth on the surfaces of the CS, CS-GR, and the carbon felt anodes. As can be seen, the biofilm is wrapped not only on the surface, which was also observed by Baranitharan et al.[31] on PAN carbon felt electrode surface, but also on the cellular wall for the CS anode (as shown in Fig. 5(a)). This indicates that the open-celled scaffold structure can provide sufficient substrate transport in the CS anode, which is not hindered by *E. coli* bacteria growth. So 3D biofilm is formed and internal colonization of *E. coli* bacteria is maintained, which is consistent with the aforementioned high hydrophilicity. As can be clearly seen in Fig. 5(b), the CS-GR anode exhibits more intense biofilm on the surface and cellular wall compared with the CS anode. Moreover, more rough surfaces stimulate the easier formation of nanowires (as marked by arrows), which facilitate the extracellular electron transfer between the bacteria and anode. The nanowires interwine each other and tether *E. coli* bacteria to the anode, facilitating the maintenance of the stable biofilm and a probable extracellular electron transfer involving path B illustrated in Fig. S1.[40–43] However, scarce *E. coli* bacteria are observed on the surface of the carbon felt anode (Fig. 5(c)), not to mention its inner surface, which results from its poor biocompatibility.

The electrochemical behaviour of potassium ferricyanide at three kinds of anodes, which reflects the reversibility and stability of the anodes, is shown in Fig. 6. A couple of well-defined redox peaks attributed to the redox reaction of ferricyanide can be directly observed. Based on the Nernst equation, if potential separation between the anodic and cathodic peaks ($\Delta E_p = E_{pa} - E_{pc}$) $> 59/n$ (unit: mv) at 25°C (where n is the number of the charge transfer, and n=1 for potassium ferricyanide reaction), the anode is quasi-reversible. The smaller the ΔE_p is, the more reversible the anode is. This is generally used as the criteria for evaluating a degree of reversibility for anodes. As can be calculated from Fig. 6, the ΔE_p for the three anodes are $>$ 59 mV, demonstrating their suitability and quasi-reversible behaviour for extracellular electron transfer from mediators or shuttles metabolized by *E. coli* bacteria to the anode, involving path C for electron transfer in Fig. S1. The CS-GR anode has lower value of ΔE_p compared to CS anode, indicating that the former with aforementioned larger specific surface area possesses more quasi-reversible behaviour. The charge capacities calculated from the results of CVs (inset in Fig. 6) further confirm that the CS-GR anode possesses the maximum value of active reaction area proportional to the anode surface area, which is expected to provide the MFCs with superior performance.

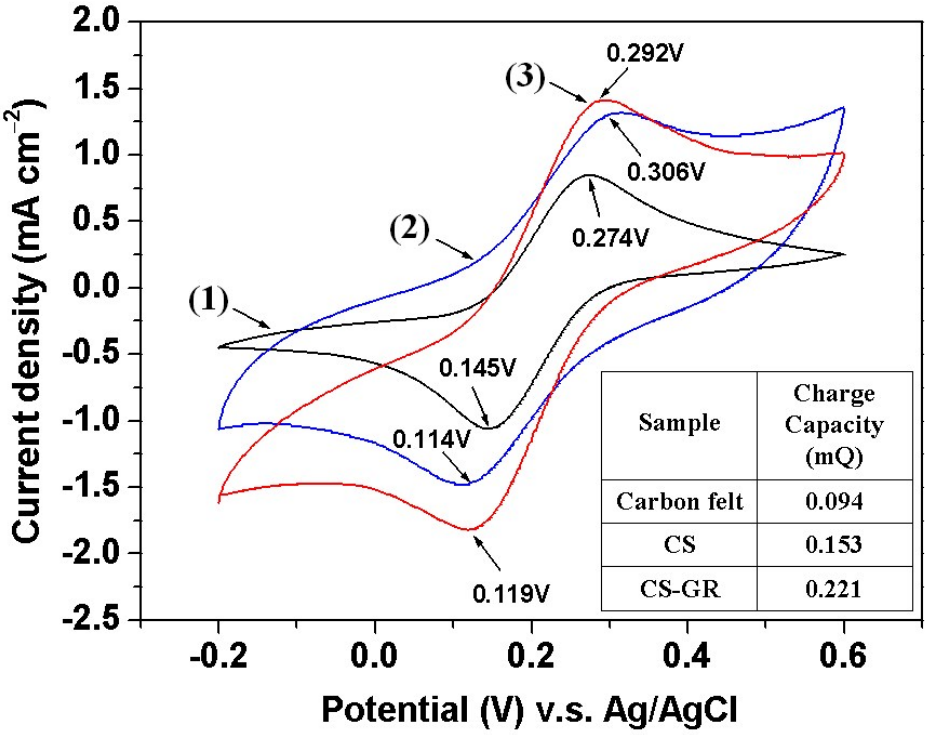

Fig. 6 Cyclic voltammograms of (1) carbon felt, (2) CS, and (3) CS-GR anodes in 5 mM $K_3Fe(CN)_6$ prepared in 100 mM KCl buffer. The scan rate was 30 mV s^{-1}.

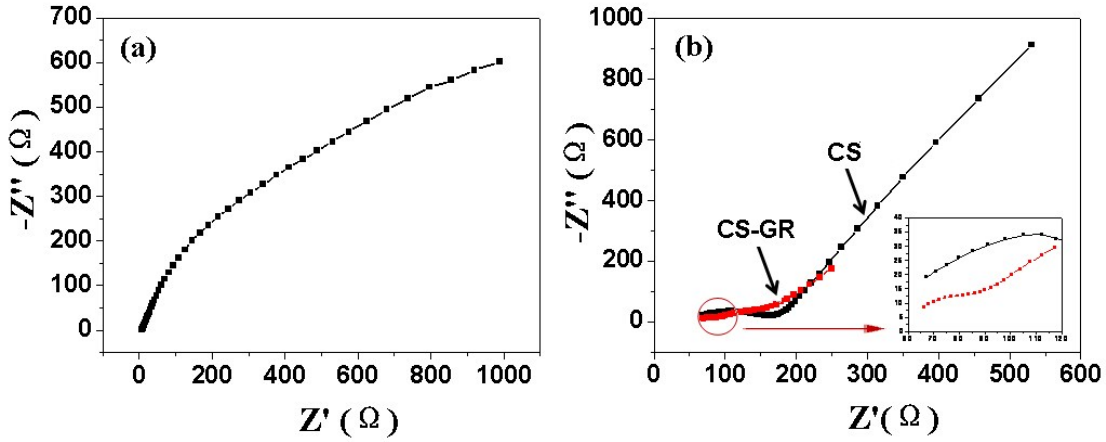

Fig. 7 Nyquist curves of (a) carbon felt anode and (b) CS and CS-GR anodes in MFCs obtained via electrochemical impedance spectroscopy tests.

3.3 Electrochemical impedance spectra of anodes

To further verify the increased interfacial interactions between the biofilm and developed anodes, which are embodied by the internal resistance of MFCs, EIS tests were conducted. The charge transfer resistance is indicated by the diameter of the first semicycle in the Nyquist curve.[44] Fig. 7 illustrates the Nyquist curves of the CS and CS-GR anodes in MFCs using 2 g L^{-1} glucose as substrate, with comparison to that of the carbon felt anode. As shown in Fig. 7, the charge transfer resistance of the carbon felt anode in the

MFC is about 1600 Ω, whereas that of the CS anode is about 130 Ω. Much lower charge transfer resistance results from the 3D open-celled scaffold structure (as shown in Fig. 2(c)) and hydrophilic –C=N group (as shown in Fig. 3). The 3D open-celled scaffold structure facilitates the substrate transfer, which is beneficial to the bacteria colonization inside the anode. Meanwhile, better hydrophilicity results in easier biofilm formation. Hence, the bacteria-fermented electron can be more easily transferred from the bacteria to anode for further suppressing the charge transfer resistance. The CS-GR anode in the MFC exhibits a charge transfer resistance as low as about 40 Ω, which is due to large charge capacity (shown in Fig. 6) and active reaction area of the CS-GR anode.[45]

3.4 Performance of MFCs

To evaluate the performance of the novelly developed open-celled scaffold anodes, they were assembled in cubic single-chamber MFCs for discharge tests. The MFC with a carbon felt anode was also assembled for comparison. Fig. 8 shows the power densitys of the MFCs with different anodes, and Table 2 summarizes the main parameters obtained from discharge tests. From Fig. 8 and Table 2, the maximum current density achieved by the MFC with the CS anode is 101% higher than that achieved by the carbon felt anode under identical condition. Much better performance of the MFC with the CS anode is attributed to much lower charge transfer resistance mentioned above. The MFC with the CS-GR anode exhibits the maximum current density of 2.91 A m^{-2} and the maximum power density of 30.7 mW m^{-2}. The latter is 28.5% higher than that with the carbon felt. These data strongly suggest that the novel CS-GR anode enables superior performance of the MFC, which is attributed to the 3D open-celled scaffold structure with –C=N group facilitating the extracellular electron transfer involving paths A and B (shown in Fig. S1) and the quasi-reversible property facilitating the extracellular electron transfer involving path C (Fig. S1).

Table 2 Main parameters of MFCs with different anodes

Anode	Internal resistance (Ω)	Maximum power density (mW m^{-2})	Maximum current density (A m^{-2})
Carbon felt	391	23.9	1.01
CS	102	25.2	2.03
CS-GR	73	30.7	2.91

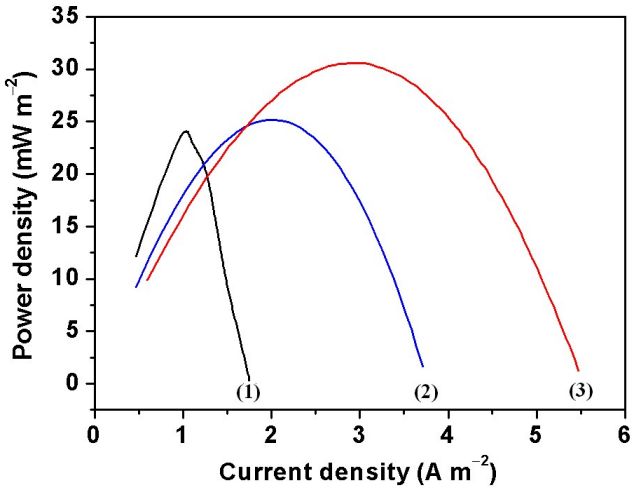

Fig. 8 Power densitys of cubic MFCs with (1) carbon felt, (2) CS, and (3) CS-GR anodes.

4. Conclusions

A novel 3D open-celled carbon scaffold (CS) anode was prepared by using supercritical carbon dioxide as the physical foaming agent from cheap polyacrylonitrile precursor for microbial fuel cell (MFC). The open-celled scaffold structure provides sufficient substrate transport and internal colonization of *E. coli* bacteria in the CS anode to form 3D biofilm. Meanwhile, the remained –C=N group after carbonization also provides the CS anode with good hydrophilicity and biocompatibility. The quasi-reversible property of the CS anode facilitating the direct extracellular electron transfer from bacteria to the anode through mediators or shuttles contributes excellent electrical conductivity to the anode. Compounded with graphite, the CS-GR anode owns all the aforementioned characteristics, and most importantly, its increased specific surface area and active reaction area provide the MFC with superior performance. This work demonstrates that the novel 3D open-celled CS-GR anode offers a new practical platform for the development of high-performance MFC anodes on a large scale.

Acknowledgements

Financial support provided by the National Natural Science Foundation of China (11172105) is gratefully acknowledged.

References

1 B. E. Logan and J. M. Regan, *Environ. Sci. Technol.*, 2006, **40**, 5172–5180.
2 L. M. Tender, C. E. Reimers, H. A. Stecher, D. E. Holmes, D. R. Bond, D. A. Lowy, K. Pilobello, S. J. Fertig and D. R. Lovley, *Nat. Biotechnol.*, 2002, **20**, 821–825.
3 O. Schaetzle, F. Barrière and U. Schröder, *Energy Environ. Sci.*, 2009, **2**, 96–99.
4 A. E. Franks, K. P. Nevin, H. F. Jia, M. Izallalen, T. L. Woodard and D. R. Lovley, *Energy Environ. Sci.*, 2009, **2**, 113–119.
5 X. X. Cao, X. Huang, P. Liang, N. Boon, M. Z. Fan, L. Zhang and X. Y. Zhang, *Energy Environ. Sci.*, 2009, **2**, 498–501.
6 H. Liu, R. Ramnarayanan and B. E. Logan, *Environ. Sci. Technol.*, 2004, **38**, 2281–2285.
7 H. Liu and B. E. Logan, *Environ. Sci. Technol.*, 2004, **38**, 4040–4046.
8 G. C. Gil, I. S. Chang, M. Kim, J. K. Jang, H. S. Park and H. J. Kim, *Biosens. Bioelectron.*, 2003, **18**, 327–334.
9 B. E. Logan and J. M. Regan, *Trends Microbiol.*, 2006, **14**, 512–518.
10 B. E. Logan and J. M. Regan, *Environ. Sci. Technol.*, 2006, **40**, 5172–5180.

11 D. K. Daniel, B. D. Mankidy, K. Ambarish and R. Manogari, *Int. J. Hydrogen. Energy.*, 2009, **34**, 7555–7560.
12 D. R. Lovley, *Nat. Rev. Microbiol.*, 2006, **4**, 497–508.
13 L. T. Angenent and M. A. Rosenbaum, *Biofuels*, 2013, **4**, 131–134.
14 S. A. Patil, K. Górecki, C. Hägerhäll and L. Gorton, *Energy Environ. Sci.*, 2013, **6**, 2626–2630.
15 X. Xie, L. B. Hu, M. Pasta, G. F. Wells, D. S. Kong, C. S. Criddle and Y. Cui, *Nano Lett.*, 2011, **11**, 291–296.
16 Y. Q. Wang, B. Li, L. Z. Zeng, D. Cui, X. D. Xiang and W. S. Li, *Biosens. Bioelectron.*, 2013, **41**, 582–588.
17 H. Liu, S. A. Cheng, L. P. Huang and B. E. Logan, *J. Power Sources*, 2008, **179**, 274–279.
18 X. Wang, S. A. Cheng, Y. J. Feng, M. D. Merrill, T. Saito and B. E. Logan, *Environ. Sci. Technol.*, 2009, **43**, 6870–6874.
19 B. E. Logan, Microbial Fuel Cells, John Wiley and Sons, Inc., Hoboken, New Jersey, 2008, p. 63.
20 Q. Deng, X. Y. Li, J. E. Zuo, A. Ling and B. E. Logan, *J. Power Sources*, 2010, **195**, 1130–1135.
21 H. Liu, R. Ramnayanan and B. E. Logan, *Environ. Sci. Technol.*, 2004, **38**, 2281–2285.
22 K. Swades, H. Chaud and D. R. Lovley, *Nat. Biotechnol.*, 2003, **21**, 1229–1232.
23 X. Xie, M. Ye, L. Hu, N. Liu, J. McDonough, W. Chen, H. C. Alshareef, S. Criddle and Y. Cui, *Energy Environ. Sci.*, 2012, **5**, 5265–5270.
24 X. Xie, G. Yu, N. Liu, Z. Bao, C. Criddle and Y. Cui, *Energy Environ. Sci.*, 2012, **5**, 6862–6866.
25 Y. Yong, X. Dong, M. Chan-Park, H. Song and P. Chen, *ACS Nano*, 2012, **6**, 2394–2400.
26 G. T. Howard, *Int. Biodeterior. Biodegrad.*, 2002, **49**, 245–252.
27 S. Cheng and B. E. Logan, *Electrochem. Commun.*, 2007, **9**, 492–496.
28 Y. Feng, Q. Yang, X. Wang and B. E. Logan, *J. Power Sources*, 2010, **195**, 1841–1844.
29 M. Picot, L. Lapinsonnière, M. Rothballer and F. Barrière, Biosens. *Bioelectron.*, 2011, **28**, 181–188.
30 Y. Yuan, B. Zhao, Y. Jeon, S. Zhong, S. Zhou and S. Kim, *Bioresour. Technol.*, 2011, **102**, 5849–5854.
31 E. Baranitharan, M. R. Khan, D. M. R. Prasad and J. B. Salihon, *Water Air Soil Pollut*, 2013, **224**, 1533.
32 S. K. Nataraj, K. S.Yang and T. M. Aminabhavi, *Prog. Polym. Sci.*, 2012, **37**, 487–513.
33 A. Malkin, S. Ilyin, T. Roumyantseva and V. Kulichikhin, *Macromolecules*, 2013, **46**, 257–266.
34 L. X. Zhang, C. S. Liu, L. Zhuang, W. S. Li, S. G. Zhou and J. T. Zhang, *Biosens. Bioelectron.*, 2009, **24**, 2825–2829.
35 L. Q. Xu and H. X. Huang, *Ind. Eng. Chem. Res.*, 2014, **53**, 2277–2286.
36 H. X. Huang and H. F. Xu, *Polym. Adv. Technol.*, 2011, **22**, 822–829.
37 H. N. Friedlander, L. H. Peebles Jr., J. Brandrup and J. R. Kirby, *Macromolecules*, 1968, **1**, 79–86.
38 S. A. Patil, S. Chigome, C. Hägerhäll, N. Torto and L. Gorton, *Bioresour. Technol.*, 2013, **132**, 121–126.
39 S. Q. Ci, Z. H. Wen, J. H. Chen and Z. He, *Electrochem. Commun.*, 2012, **14**, 71–74.
40 G. Reguera, K. D. McCarthy, T. Mehta, J. S. Nicoll, M. T. Tuominen and D. R. Lovley, *Nature*, 2005, **435**, 1098–1101.
41 N. S. Malvankar, M. Vargas, K. P. Nevin, A. E. Franks, C. Leang, B. C. Kim, K. Inoue, T. Mester, S. F. Covalla, J. P. Johnson, V. M. Rotello, M. T. Tuominen and D. R. Lovley, *Nat. Nanotechnol.*, 2011, **6**, 573–579.
42 M. Y. El-Naggar, G. Wanger, K. M. Leung, T. D. Yuzvinsky, G. Southam, J. Yang, W. M. Lau, K. H. Nealson and Y. A. Gorby, *Proc. Natl. Acad. Sci. U. S. A.*, 2010, **107**, 18127–18131.
43 Y. A. Gorby, S. Yanina, J. S. McLean, K. M. Rosso, D. Moyles, A. Dohnalkova, T. J. Beveridge, I. S. Chang, B. H. Kim, K. S. Kim, D. E. Culley, S. B. Reed, M. F. Romine, D. A. Saffarini, E. A. Hill, L. Shi, D. A. Elias, D. W. Kennedy, G. Pinchuk, K. Watanabe, S. Ishii, B. Logan, K. H. Nealson and J. K. Fredrickson, *Proc. Natl. Acad. Sci. U. S. A.*, 2006, **103**, 11358–11363.
44 Z. He and F. Mansfeld, *Energy Environ. Sci.*, 2009, **2**, 215–219.
45 C. I. Torres, A. K. Marcus and B. E. Rittmann, *Biotechnol. Bioeng.*, 2008, **100**, 872–881.

